Structure of Mini-B, a Functional Fragment of Surfactant Protein B, in Detergent Micelles[†,‡]

Muzaddid Sarker,[§] Alan J. Waring,[||,⊥] Frans J. Walther,[∞,▽] Kevin M. W. Keough,[▽] and Valerie Booth*[,§,▽]

Departments of Biochemistry and Physics & Physical Oceanography, Memorial University of Newfoundland, St. John's, Newfoundland, Canada A1B 3X9, Department of Medicine, UCLA School of Medicine, Los Angeles, California 90095, Los Angeles Biomedical Research Institute at Harbor−UCLA Medical Center, Torrance, California 90502, and Department of Pediatrics, Leiden University Medical Center, 2333 ZA Leiden, The Netherlands

Received June 14, 2007; Revised Manuscript Received July 26, 2007

ABSTRACT: Surfactant protein B (SP-B) is essential for normal lung surfactant function, which is in itself essential to life. However, the molecular basis for SP-B's activity is not understood and a high-resolution structure for SP-B has not been determined. Mini-B is a 34-residue peptide with internal disulfide linkages that is composed of the N- and C-terminal helical regions of SP-B. It has been shown to retain similar activity to full-length SP-B in certain in vitro and in vivo studies. We have used solution NMR to determine the structure of Mini-B in the presence of micelles composed of the anionic detergent sodium dodecyl sulfate (SDS). Under these conditions, Mini-B forms two α-helices connected by an unstructured loop. Mini-B possesses a strikingly amphipathic surface with a large positively charged patch on one face of the peptide and a large hydrophobic patch on the opposite face. A tryptophan side chain extends outward from the peptide in a position to interact with lipids at the polar/apolar interface. Interhelix interactions are stabilized by both disulfide bonds and by interleaving of hydrophobic side chains from the two helices.

Surfactant protein B (SP-B[1]) is an essential component of lung surfactant, a material that is indispensable for normal breathing. Lung surfactant is a mixture of lipids and proteins that lines the air-water interface in alveoli. One of its main functions is to drastically reduce the surface tension at the air-water interface, thus preventing alveolar collapse during expiration and reducing the work of breathing (1, 2). Lung surfactant components are also important in the innate immune response to microbes in the lungs (3).

Deficiency or inactivation of lung surfactant leads to potentially fatal respiratory disorders such as neonatal respiratory distress syndrome (NRDS) in premature newborns (*4*) and acute respiratory distress syndrome (ARDS) in adults with acute injury and illness (*5*). Development of lung surfactant replacement treatments in the early 1990s greatly improved the outlook for NRDS (*6*), but successful treatment of ARDS with endogenous surfactant has proved more challenging, probably because the conditions that lead to ARDS in the first place lead to rapid deactivation of the replacement surfactant (*7*). Clinical trials have shown artificial surfactants to be much more effective if they include the proteins SP-B or SP-C, as compared to protein-free preparations (*8*). The requirement for SP-B's presence in effective surfactant replacement therapy is in keeping with the lethality of hereditary SP-B deficiency in humans (*9*) and knockout mice (*10*). Improvement of surfactant replacement preparations, for example, to avoid the use of animal-derived surfactant and to improve its activity in the context of ARDS, is hampered by a lack of understanding of the structural bases for the activity of the lung surfactant proteins.

Lung surfactant is synthesized and secreted into the alveolar fluid by epithelial type II pneumocytes (*11*). The composition of lung surfactant varies among different vertebrates and also throughout the physiological develop-

[†] We acknowledge financial support from the Canadian Institutes of Health Research and the National Institutes of Health (Grant R01 HL55534) and salary support for V.B. from the Parker B. Francis Foundation.

[‡] The structures of Mini-B have been deposited in the Protein Data Bank as entries 2JOU (in hexafluoro-2-propanol) and 2DWF (in sodium dodecyl sulfate micelles). The chemical shifts of Mini-B have been deposited in the BMRB data bank as entry 6741.

* To whom correspondence should be addressed: phone (709) 737-4523; fax (709) 737-2422; e-mail vbooth@mun.ca.

[§] Department of Physics and Physical Oceanography, Memorial University of Newfoundland.

[||] UCLA School of Medicine.

[⊥] Los Angeles Biomedical Research Institute at Harbor−UCLA Medical Center.

[∞] Leiden University Medical Center.

[▽] Department of Biochemistry, Memorial University of Newfoundland.

[1] Abbreviations: SP-A, SP-B, SP-C, and SP-D, surfactant proteins A, B, C, and D, respectively; NRDS, neonatal respiratory distress syndrome; ARDS, acute respiratory distress syndrome; PG, phosphatidylglycerol; DPPC, dipalmitoylphosphatidylcholine; CD, circular dichroism; FTIR, Fourier transform infrared; NMR, nuclear magnetic resonance; HPLC, high-performance liquid chromatography; MALDI-TOF, matrix-assisted laser desorption/ionization time of flight; HFIP, hexafluoro-2-propanol; SDS, sodium dodecyl sulfate; DSS, 2,2-dimethyl-2-silapentane-5-sulfonate sodium salt; HSQC, heteronuclear single quantum correlation; TOCSY, total correlation spectroscopy; NOE, nuclear Overhauser effect; NOESY, nuclear Overhauser effect spectroscopy; DOSY, diffusion-ordered spectroscopy; ppm, parts per million; CSI, chemical shift index; RMSD, root-mean-square deviation; MUN, Memorial University of Newfoundland; NANUC, National High Field NMR Centre; PDB, Protein Data Bank.

10.1021/bi7011756 CCC: $37.00
Published on Web 09/11/2007

ment of a particular species (*12*). For humans (and most mammals), phospholipids make up the bulk of surfactant materials (~80% by weight), with ~10% neutral lipids and ~10% proteins (*13*). Surfactant proteins A and D (SP-A and SP-D) are water-soluble and primarily involved in immunological functions (*14*, *15*). The other two surfactant proteins B and C (SP-B and SP-C) are hydrophobic and exhibit high surface activity (*16*, *17*). Out of these four proteins, SP-B accounts for only about 1.5% of the total surfactant weight but is essential for survival (*18*). Hereditary deficiency of SP-B is lethal in humans (*9*) and in knockout mice (*10*), and antibodies against SP-B cause respiratory distress syndrome in vivo (*19*). Biophysical studies have demonstrated a number of in vitro activities of SP-B including membrane binding, membrane lysis, membrane fusion, promotion of lipid adsorption to air−water surfaces, stabilization of monomolecular surface films, and respreading of films from collapsed phases (*16*). However, it is not clear which of these activities, if any, underlies SP-B's crucial contributions to lung function in vivo.

In the mammalian lung, SP-B is found as a covalently linked homodimer with a monomeric molecular mass of 8.7 kDa (*20*). The SP-B gene is first transcribed and translated into a 381 amino acid precursor, which is then cleaved proteolytically to produce the mature protein, 79 residues in length in humans (*16*). A large portion (52%) of SP-B's amino acids are hydrophobic (Ala, Val, Leu, Ile, Phe, and Trp). The protein also exhibits a strong cationic profile with nine positively charged and two negatively charged amino acids, yielding a net charge of +7 at neutral pH. There are seven cysteines, six of which form three intrachain disulfide bridges and the remaining one of which forms the interpeptide bond responsible for dimerization.

Given SP-B's positive charge, it seems likely that electrostatic interactions between SP-B and the negatively charged lipid components of lung surfactant are part of its physiological function. Indeed, certain studies have found that SP-B preferentially binds anionic phospholipids such as phosphatidylglycerol (PG) in surface monolayers of surfactant films (*21*, *22*), as well as in multilamellar vesicles (*23*). Upon compression, films composed of SP-B and anionic lipids form buckled structures that remain attached to the monolayer (*24*). During subsequent expansion of the film at a lower surface pressure, the buckled structures are rapidly reincorporated into the film to re-form a flat monolayer (*25*, *26*). SP-B is also essential for the formation of SP-A−dipalmitoylphosphatidylcholine (DPPC) tubular myelin structures that have been proposed to be responsible for transporting lipids from aqueous subphase to the surface monolayer (*27*, *28*). All these observations suggest that SP-B's critical contributions to lung surfactant function are made via facilitating large-scale lipid rearrangements and stabilizing structures required for interfacial adsorption, film stability, and respreading capacities of lung surfactant. However, the details of SP-B's function in the lungs are not yet well understood, in part because SP-B's three-dimensional structure has not been determined.

SP-B belongs to the saposin protein superfamily (*29*, *30*), several members of which have known high-resolution structures. Saposin A [PDB entry 2DOB] (*31*), saposin B [PDB entry 1N69] (*32*), saposin C [PDB entry 1SN6] (*33*), NK-lysin [PDB entry 1NKL] (*34*), amoebapore A [PDB entry 1OF9] (*35*), and the saposin-like protein granulysin [PDB entry 1L9L] (*36*) all display a predominantly α-helical conformation, although the extent of the helices and the way the helices pack together vary from protein to protein. In all the saposin family proteins, three intrapeptide disulfide bonds are formed by six conserved cysteine residues, which define a characteristic fold that has been conserved for an estimated 300 million years (*37*). Thus, SP-B is expected to possess four or five α-helices connected by three disulfide bonds. The helical content has been verified by circular dichroism (CD) and Fourier transform infrared (FTIR) spectroscopy of native SP-B in both lipid and organic solvent environments (*38*−*40*).

Fragments of SP-B containing individual helices or pairs of helices have been shown to retain significant activity when compared to the full-length protein. Surfactant preparations containing synthetic peptides representing either N- or C-terminal helical segments of SP-B enhance oxygenation and lung compliance in surfactant-deficient animal models (*41*, *42*). A 25-residue N-terminal segment of SP-B (SP-B_{1-25}) facilitates dynamic respreading (*43*) and improves lung function in premature rabbits and lavaged rats (*44*). Peptides based on the C-terminal domain also induce in vitro and in vivo surfactant activities that, at least partially, simulate those of the native protein (*41*, *45*, *46*). The N-terminal half of SP-B consisting of residues 1−37 promotes rapid liposome fusion, while a shorter peptide containing residues 7−22 is sufficient for liposome lysis (*47*). KL4 (a component of Surfaxin), a 21-residue peptide designed by use of the hydrophobic and hydrophilic repeats of SP-B_{57-63} as a molecular template, has shown some promise as a bronchoalveolar lavage for improving lung function in meconium aspiration syndrome (*48*).

Mini-B is a 34-residue construct based on the sequence of the N- and C-terminal predicted helices of SP-B (*49*). Like full-length SP-B, Mini-B possesses a net charge of +7. Mini-B also possesses four of the six conserved cysteines that define the saposin fold and thus, in its oxidized form, has two disulfide bridges linking the two helices. Surfactant-deficient rats treated with model surfactant preparations containing Mini-B attain oxygenation and lung compliance values as good as or better than those achieved in the presence of native SP-B (*49*). It should be noted that in this study the surfactant material was added exogenously and so the findings cannot speak to any additional requirements that may be needed for SP-B in naturally produced surfactant, which must somehow travel from the lamellar bodies secreted by type II alveolar cells to the air−water interface. All the same, high-resolution structural studies of Mini-B can be expected to unveil at least some of the critical structural features that underlie the activity of SP-B.

To date, structures of two peptides representing the terminal regions of SP-B have been determined with atomic resolution by nuclear magnetic resonance (NMR). The structure of an N-terminal peptide (SP-B_{11-25}) has been determined in methanol [PDB entry 1KMR] (*50*). The structure of a C-terminal peptide (SP-B_{63-78}) has been determined in the fluorinated alcohol hexafluoro-2-propanol (HFIP) [PDB entry 1RG4] and in lipid-mimicking sodium dodecyl sulfate (SDS) micelles [PDB entry 1RG3] (*51*). In this study, we have used solution NMR to study the high-resolution structures of Mini-B in both HFIP and SDS

micelles. The SDS micelles supply an anionic, lipidlike environment that provides a reasonable mimetic of SP-B's physiological environment. HFIP does not provide a very physiologically relevant environment, but the HFIP NMR frequency assignments were necessary in order to obtain the assignments in SDS and hence allow the structure to be determined.

MATERIALS AND METHODS

Peptide Synthesis and Purification. Mini-B (amino acid sequence −CWLCRALIKRIQAMIPKGGRMLPQLVCR-LVLRCS) was produced by solid-phase chemical synthesis via *O*-fluorenylmethyloxycarbonyl (Fmoc) chemistry with partial ^{15}N-labeling. ^{15}N-Leucine was incorporated at positions 3, 7, 22, 25, 29, and 31; ^{15}N-alanine, at residues 6 and 13; and ^{15}N-glycine, at residue 18. Two versions of the peptide were produced, oxidized Mini-B (Mini-B_{ox}), with disulfide bonds between C1−C33 and C4−C27, and reduced Mini-B (Mini-B_{red}), without the disulfide bonds. Intramolecular disulfide linkages were directed by selective deprotection of the Cys residues at amino acid positions 1 and 33 via trityl side-chain protecting protocols and at positions 4 and 27 by use of acetamidomethyl groups (*49*). The disulfide linkages were formed by air-mediated oxidation of the peptide in structure-promoting solvents (*49*). Fmoc amino acids and coupling agents were purchased from AnaSpec. The ^{15}N-labeled amino acids were purchased from Cambridge Isotope Laboratories and converted to their Fmoc derivatives by AnaSpec. Organic solvents and other reagents used for the synthesis and purification were high-performance liquid chromatography (HPLC) grade or better (Fisher Scientific, Aldrich Chemical). The peptide was synthesized at a 0.25 mmol scale in an ABI 431A peptide synthesizer configured for FastMoc double-coupling cycles for all residues for optimum yield (*52*). A prederivatized *N*-Fmoc-*O*-*tert*-butylserine HMP resin (AnaSpec) was used to assemble the peptide after synthesis. Deprotection and cleavage of the peptide from the resin were carried out by use of a trifluoroacetic acid (TFA)/thioanisole/EDTA/phenol/water mixture (10/0.5/0.25/0.5/0.5 by volume) followed by cold precipitation with *tert*-butyl ether. The crude product was then purified by preparative reverse-phase HPLC in a Vydac C-18 column by use of a water/acetonitrile linear gradient with 0.1% trifluoroacetic acid as the ion-pairing agent. The molecular weight of the peptide was confirmed by fast atom bombardment or MALDI-TOF mass spectrometry. The purity (>95%) of the final product was determined by analytical HPLC. The purified peptide was lyophilized and stored at 4 °C.

NMR Sample Preparation. The sample of Mini-B_{red} in hexafluoro-2-propanol (HFIP) was prepared by dissolving 1.5 mM peptide in 40% HFIP (98% deuterated), 50% H_2O, and 10% D_2O with 0.4 mM 2,2-dimethyl-2-silapentane-5-sulfonate (DSS). For the sample of Mini-B_{ox} in sodium dodecyl sulfate (SDS) micelles, 1.5 mM peptide and 150 mM SDS (98% deuterated) were dissolved in 90% H_2O and 10% D_2O with 0.4 mM DSS and 0.2 mM NaN_3. All deuterated chemicals were purchased from Cambridge Isotope Laboratories. The pH for both samples was set at 5 by use of NaOH and HCl solutions (without taking the isotope effects into account). This pH was chosen in order to be sure that Mini-B_{red} remained reduced and because it was preferable to obtain the NMR spectra in a pH region where the amide proton/deuteron exchange rate is relatively slow.

NMR Data Collection. Solution NMR experiments were performed on Bruker Avance 500, 600, and 700 MHz spectrometers (500 and 600 MHz at Memorial and 700 MHz at Health Canada) and Varian INOVA 500 and 800 MHz spectrometers (at NANUC). All the spectrometers were equipped with *z*-gradients. The 1D ^{1}H experiments used presaturation, ^{15}N−^{1}H HSQC experiments used water flip-back and TOCSY, and NOESY and DOSY experiments used water-gate water suppression techniques. Initial 1D ^{1}H and 2D ^{15}N−^{1}H HSQC experiments were done for both samples at three different temperatures (15, 25, and 35 °C for Mini-B_{red} in HFIP at 700 MHz; 25, 35, and 45 °C for Mini-B_{ox} in SDS at 500 MHz) to evaluate the temperature dependence of the peptide conformation. It was observed that the peptide exhibited improved conformational homogeneity and less signal overlap in HFIP at 15 °C and in SDS at 45 °C. Therefore, all subsequent NMR experiments were conducted at these temperatures. Scalar-coupled spin systems were identified by use of 2D TOCSY (mixing times of 45 and 80 ms for Mini-B_{red} and Bruker 700 MHz; 80 ms for Mini-B_{ox} and Bruker 500 MHz). NOE data for structure restraints were obtained from 2D NOESY (mixing times 100, 200, and 300 ms for Mini-B_{red} and Bruker 700 MHz; 200 ms for Mini-B_{ox} and Bruker 500 MHz). Three-dimensional ^{15}N-edited TOCSY (only for Mini-B_{ox}; mixing time 80 ms for Bruker 500) and 3D ^{15}N-edited NOESY (mixing time 200 ms for Mini-B_{red} and Bruker 500 MHz and for Mini-B_{ox} and Varian 800 MHz) were used to resolve overlapped peaks.

Diffusion constants were obtained from 2D DOSY data acquired with pulsed field gradient (PFG) NMR (*53*) on a Bruker 600 MHz spectrometer. The samples used were SDS micelles alone (at 150 mM concentration; pH 5, temperature 25 °C) and SDS−peptide complexes (150 mM SDS with 1.5 mM Mini-B_{ox}; pH 7, temperature 37 °C). The pulse sequence for diffusion measurement used stimulated echo (*54*) with bipolar gradient pulses, followed by 3−9−19 pulse for water suppression (*55*). Two-dimensional DOSY spectra were collected in 32 steps, attenuating signals to about 5% of the initial value by increasing the gradient strength from 2% to 95% of the maximum amplitude, for a constant diffusion time of 100 ms and an optimized gradient pulse length of 4 ms.

Data Processing and Structure Calculation. The NMR spectra were processed with NMRPipe 2.2 (*56*) and the frequency assignments were made with Sparky 3.110 (*57*). The NOESY spectra of 200 ms mixing time were used for generating the distance restraints for the structure calculation. The NOEs were classified into strong, medium, and weak categories depending on the peak intensities (heights) and assigned distance ranges accordingly (1.8−2.8 Å for strong, 1.8−3.4 Å for medium, and 1.8−5.0 Å for weak). Dihedral angle and hydrogen bond restraints were added for residues that could clearly be identified as α-helical from local NOE patterns, which were residues 3−14 and 23−32. Hydrogen bond restraints were set to 1.7−2.4 Å for $O_i\cdots HN_{i+4}$ and 2.5−3.5 Å for $O_i\cdots N_{i+4}$ and dihedral angles were set to $\phi = -60° \pm 30°$ and $\psi = -40° \pm 40°$ for these residues. Table 1 summarizes the experimental restraints used in the structure calculation. Structures of Mini-B were calculated

Table 1: Restraints for Mini-B Structure Calculation

restraints	no.
total NOE distance restraints	638
unambiguous	613
intraresidue	339
sequential ($\|i-j\|=1$)	158
medium-range ($\|i-j\|\leq 5$)	110
long-range ($\|i-j\|\geq 5$)	06
ambiguous (interresidue)	25
dihedral angle restraints	44
hydrogen bond restraints	28
disulfide bonds	2

by use of the simulated annealing algorithm within CNS 1.1 (*58*). Structures were viewed by MOLMOL 2k.2 (*59*). Whenever possible, stereospecific assignments were made by use of distances derived from a preliminary structure calculation. A total of 200 structures were calculated for Mini-B_{red} in HFIP and 500 for Mini-B_{ox} in SDS. Ensembles of the 15 lowest-energy structures were retained for further analysis and deposited to the Protein Data Bank (PDB) (entries 2JOU and 2DWF, respectively).

The DOSY spectra of SDS alone and Mini-B_{ox}/SDS complex were processed by Bruker Topspin 2.0. The diffusion constants were derived from the equation for the attenuation of the signal, with the sinusoidal shape of the gradient pulse taken into account:

$$I = I_0 \exp[-(4/\pi^2)D\gamma^2 g^2 \delta^2(\Delta - \delta/4)]$$

where I is the observed signal intensity, I_0 is the unattenuated signal intensity, D is the diffusion constant (coefficient), γ is the gyromagnetic ratio of the observed nucleus ^{1}H, δ is the gradient pulse length and Δ is the diffusion time. The hydrodynamic radius was calculated from the Stokes−Einstein equation:

$$D = \frac{kT}{6\pi\eta R_H}$$

where k is the Boltzmann constant, T is the absolute temperature, η is the viscosity of the solution, and R_H is the hydrodynamic radius.

RESULTS

Mini-B is based on the N- and C-terminal predicted α-helices of human SP-B and is composed of the human sequence residues 8−25 joined to 63−78 (Figure 1) (*49*). In full-length SP-B, these two predicted helical segments are linked by a pair of cysteine−cysteine disulfide bonds. Solution NMR studies of Mini-B were performed both with and without the disulfide bonds. NMR spectra for Mini-B without the disulfide bonds, termed Mini-B_{red}, were acquired in aqueous solution with 40% HFIP, a fluorinated structure-inducing organic solvent. The structure of Mini-B with the two disulfide bonds, termed Mini-B_{ox}, was determined in SDS micelles, which provide an environment similar to the lipid−water interfacial environment in which SP-B functions in the lungs. The HFIP data sets were critical in guiding the frequency assignment of the SDS spectra, which displayed relatively broad lines and consequently significant overlap. In both cases Mini-B was produced by chemical synthesis and hence it was feasible to use only limited isotope labeling. Nine of Mini-B's 34 residues (six leucines, two alanines, and one glycine) had ^{15}N labels.

Two-dimensional ^{15}N−^{1}H HSQC spectra obtained at a variety of temperatures indicated that conformational inhomogeneity and spectral overlap were minimized at a temperature of 15 °C for Mini-B_{red} in HFIP and 45 °C for Mini-B_{ox} in SDS. Therefore, these temperatures were chosen for the structural analysis. The HSQC spectrum of Mini-B_{red} in HFIP (Figure 2A) shows nine well-dispersed peaks of comparable intensity and no weaker peaks, indicating that the peptide's conformation is homogeneous under these conditions. In SDS, the HSQC peaks for Mini-B_{ox} are much broader, as expected given the larger complex size, but at 45 °C they are well-dispersed and resolved (Figure 2B). Eight of the peaks have comparable intensity but there are also some weaker peaks present. One of the weak peaks was assigned to L3 and the other weak peaks likely arise from minor conformations of L7, G18, and L22. These spectral features are consistent with a degree of flexibility in SDS-bound Mini-B.

To probe the possibility that protein−protein interactions were responsible for the weak peaks in the HSQC of Mini-B in SDS, we also acquired HSQC spectra at lower peptide/micelle concentrations. There was no reduction in the intensity of the weak peaks as compared to the major peaks in either the 0.5 mM Mini-B_{ox}/50 mM SDS sample or the 0.1 mM Mini-B_{ox}/10 mM SDS sample (Supporting

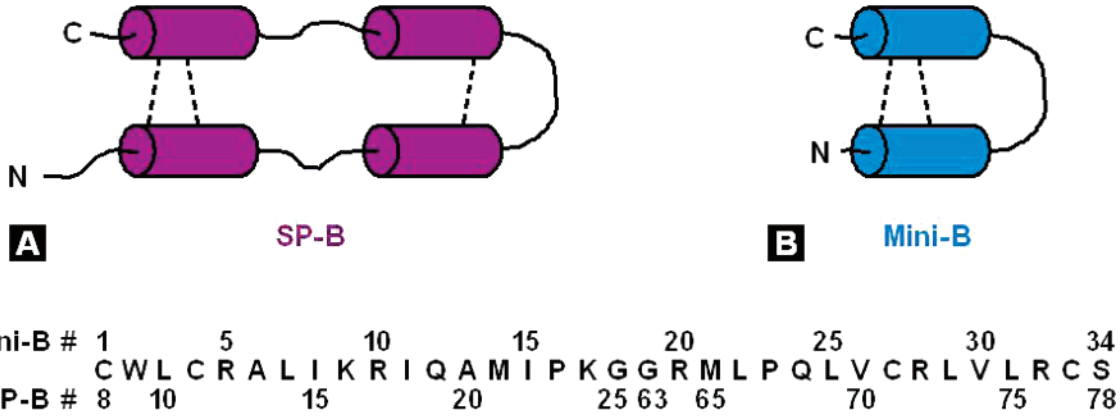

FIGURE 1: (A) Topology of SP-B predicted on the basis of the known structures of other saposin proteins. α-Helical regions are portrayed as cylinders, and disulfide bonds connecting the helices are shown by dashed lines. (B) Mini-B is constructed by connecting the helical segments at the termini of the full-length protein. The correspondence between Mini-B residue numbering and SP-B residue numbering is shown at the bottom.

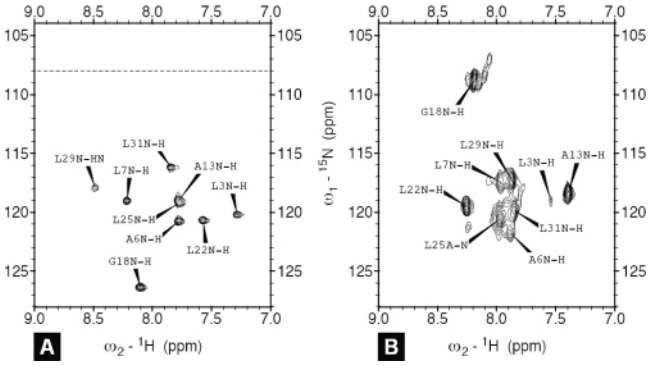

FIGURE 2: (A) ^{15}N−^{1}H HSQC spectra of Mini-B_{red} in HFIP at 15 °C. Note that the actual ^{15}N acquisition spectral width was between 108 and 128 ppm (high-field limit is shown by the dashed line) and the G18 peak has been aliased from its true frequency of 106.5 ppm. (B) ^{15}N−^{1}H HSQC spectra of Mini-B_{ox} in SDS at 45 °C. Spectra for both samples were acquired on a Bruker 500 MHz spectrometer with 16 scans. The base contour level shown for panel B is 2 times lower than the base level shown for panel A.

Information Figure 1). Hence, it does not appear that these weak peaks are the result of protein−protein binding.

Frequency assignments for Mini-B were made primarily by use of 2D ^{1}H−^{1}H TOCSY and NOESY spectra with help from ^{15}N-edited 3D experiments for the ^{15}N-labeled residues. All the expected proton resonance frequency assignments could be made for Mini-B_{red} in HFIP. There was significant overlap in the SDS spectra (Figure 3), but with the knowledge of side-chain assignments of Mini-B_{red} in HFIP, it was possible to identify the correlations to confirm frequency assignments for all but Hγ of L3, L7, and L22 of Mini-B_{ox} in SDS. NOESY peaks involving C1, W2, L3, C4, and R5 were weak and displayed only a few interresidue correlations. The relatively weak peak intensity for residues 1−5 is consistent with dynamics on an intermediate time scale involving the N-terminal region of Mini-B_{ox}. NOEs indicative of secondary structure and Hα chemical shift index (CSI) are shown in Figure 4. $H\alpha_i$−$HN_{i+3/i+4}$ NOEs and generally negative CSI values indicate an α-helical conformation for residues 3−14 and 23−32 of Mini-B_{ox} in SDS.

Although the HFIP data was primarily used to help assign the SDS data, NOE assignments and structure calculations were performed for Mini-B_{red} in HFIP (PDB entry 2JOU). The HFIP structures displayed fairly similar secondary structure to Mini-B_{ox} in SDS, although the C-terminal helix was less well defined in HFIP. The lack of disulfide bonds and the fluorinated solvent environment make the actual structures largely irrelevant to discussions of SP-B's function in the lungs and so the Mini-B_{red} in HFIP structures will not be discussed further here.

For Mini-B_{ox} in SDS micelles, the structures were calculated from 299 interresidue NOEs, plus 44 dihedral angle and 28 hydrogen bond restraints for the helical regions (Figure 5). In the ensemble of the 15 lowest energy structures, 73% of the residues were found in the most favorable region of the Ramachandran plot, the overall backbone RMSD was 0.98 Å, and the backbone RMSD of the helical regions (residues 3−14 and 23−32) was 0.78 Å. Unambiguous interhelix NOEs were observed between residues R5 and R28, L7 and P23, I8 and C27, K9 and Q24, and W2 and S34. The two helices are packed close to each other and their relative positions are almost parallel.

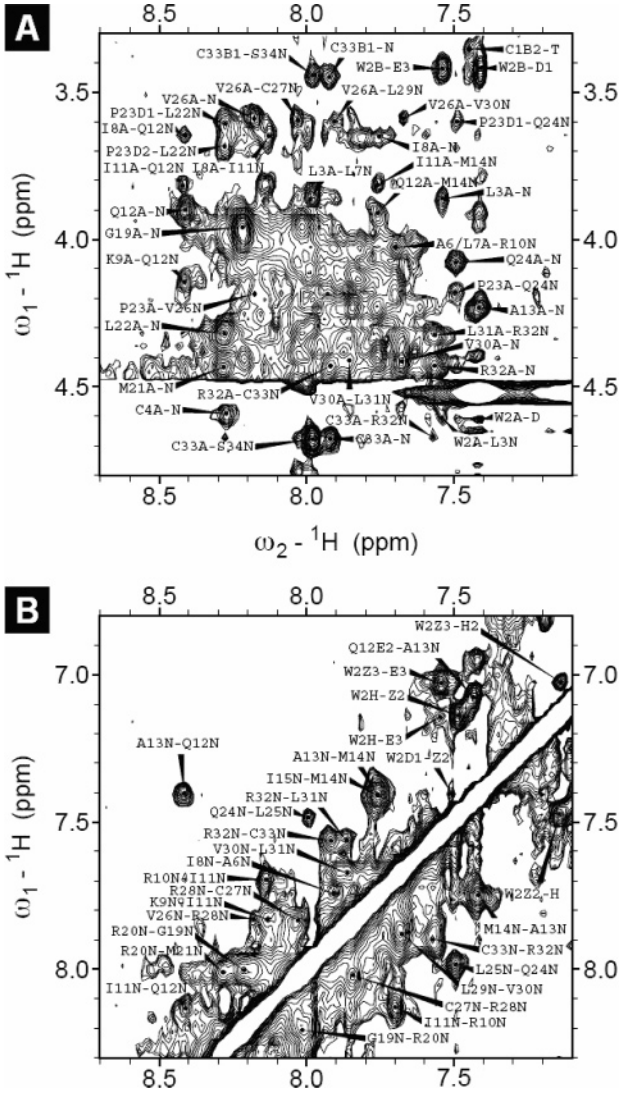

FIGURE 3: Portions of 2D NOESY spectra of Mini-B_{ox} in SDS micelles acquired on a Bruker 500 MHz spectrometer with a mixing time of 200 ms: (A) Hα−HN region and (B) HN−HN region. Note that all the peaks displayed were assigned, but for clarity, not all have been labeled.

Diffusion NMR spectra were obtained in order to provide a measure of the size of the SDS micelles in complex with Mini-B (Supporting Information Figure 2). For another project in our research group, we have measured the diffusion constant of micelles formed by 150 mM SDS to be 8.4 × 10^{-11} m^2/s (at 25 °C). By application of the Stokes−Einstein relationship, this diffusion constant corresponds to a hydrodynamic diameter of 5.8 nm. This value is consistent with small-angle neutron scattering (SANS) and small-angle X-ray scattering (SAXS) data that indicates spheroidal SDS micelles are from 4.5 to 5.6 nm in diameter for various concentrations between 65 and 600 mM (*60*−*62*). For 1.5 mM Mini-B in 150 mM SDS, we obtained a diffusion constant of 9.6 × 10^{-11} m^2/s (at 37 °C), which corresponds to a Stokes−Einstein (hydrodynamic) diameter of 6.8 nm.

DISCUSSION

Although SP-B's contributions to lung function are clearly essential for life, the mechanisms by which SP-B acts are still far from being understood. The current evidence points

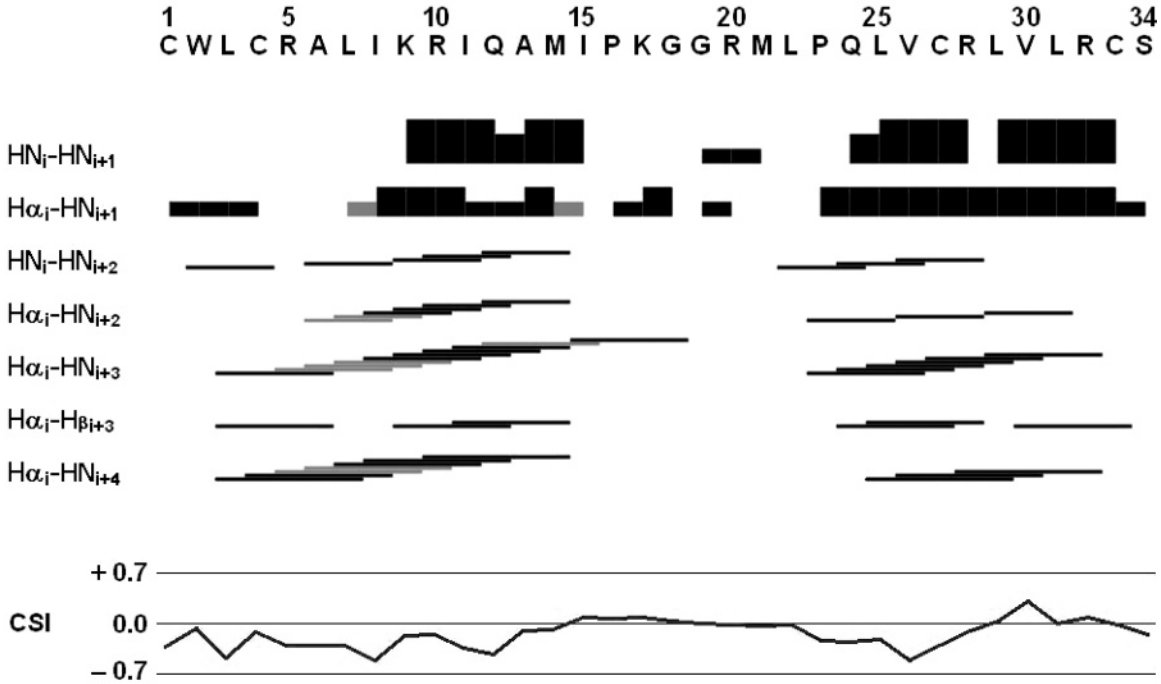

FIGURE 4: Secondary structure indicators for Mini-B_{ox} in SDS micelles. Black bars indicate unambiguously assigned NOEs, and gray bars represent ambiguous NOEs. For sequential NOEs, the height of the bar corresponds to the intensity of the NOE. The chemical shift index (CSI) for the Hα resonances is shown at the bottom. These were calculated by use of the random coil chemical shifts obtained from ref *66*.

to SP-B-induced lipid restructuring, especially through interactions with anionic lipids, as being a key part of SP-B function (*21*, *24*). In order to help reveal the structural mechanisms that underlie SP-B's function, we have performed NMR structural studies of Mini-B, a SP-B-based peptide that appears to retain at least some of the essential activities of native SP-B (*49*). Mini-B is constructed from the N- and C-terminal helical regions of human SP-B (Figure 1). It contains 34 of SP-B's 79 amino acids and also possesses the same net charge of +7 as full-length SP-B. The correspondence between the Mini-B residue numbering and the native SP-B residue numbering is shown in Figure 1; in the discussion below, residue numbers refer to Mini-B residue numbering. Mini-B and native SP-B both contain a high proportion of hydrophobic residues (Ala, Val, Leu, Ile, Phe, and Trp): 41% in Mini-B and 52% in SP-B. The distribution of the positively charged and hydrophobic residues is of high interest since this distribution defines how Mini-B and SP-B interact with lipids. One major finding of these Mini-B structural studies is that Mini-B possesses a strikingly amphipathic surface with most of the positively charged residues localized to one face of the peptide and a large hydrophobic patch on the opposite face (Figure 6A).

SP-B is a member of the saposin superfamily of proteins whose common structural features are four to five helices and three internal disulfide bonds (*31*−*35*). Mini-B contains the N- and C-terminal predicted α-helices of SP-B and also four of the six cysteine residues that form intrachain disulfide bonds in native SP-B. Thus, in the oxidized Mini-B structure presented herein, two disulfide bonds connect the two helical segments. The structure of Mini-B_{ox} was determined in the presence of SDS micelles, which provide an anionic, lipidlike environment with a hydrophobic/hydrophilic interface. NMR data was also acquired with reduced Mini-B in 40% HFIP aqueous solution and used to guide assignment of the Mini-B_{ox} in SDS spectra.

The experimental structures indicated that, in SDS, Mini-B_{ox} folds into the predicted two α-helical segments. The two helices are packed tightly together (Figure 5), with interhelical interactions stabilized by the two disulfide bonds, as well as by several hydrophobic contacts. Ile 8, Ile 11, Ile 15, Leu 22, Pro 23, Leu 25, and Leu 31 are largely buried and make interleaved contacts across the interhelix interface that appear to stabilize the interaction between the helices. Given the extensive hydrophobic contacts, it does seem plausible that some helix−helix association could occur in a nativelike lipid environment, even in the absence of disulfide bonds. This is consistent with the observation that reduced SP-B mimics the behavior of native SP-B in lipid−protein films subjected to dynamic compression−expansion cycling, but only in the presence of phosphatidylglycerol (*63*).

In water, at concentrations higher than the critical micelle concentration, the anionic detergent SDS forms micelles. These micelles are spherical structures of about 5 nm in diameter (*60*−*62*), with the hydrophobic chains on the inside and the negatively charged head group on the outside. Such micelles provide a mimic of the lipid environment in which SP-B is thought to function in the lungs. When in association with SDS micelles, Mini-B_{ox} takes on a strikingly amphipathic structure (Figure 6A). Five of the seven positively charged residues (Arg 5, Lys 9, Arg 10, Arg 28, and Arg 32) cluster into a positively charged patch on one face of the peptide. The remaining two cationic amino acids (Lys 17 and Arg 20) extend outward from the loop connecting the two helices. A large hydrophobic patch, formed mainly by residues Leu 3, Leu 7, Val 26, Leu 29, and Val 30, is located on the face opposite to the positively charged patch.

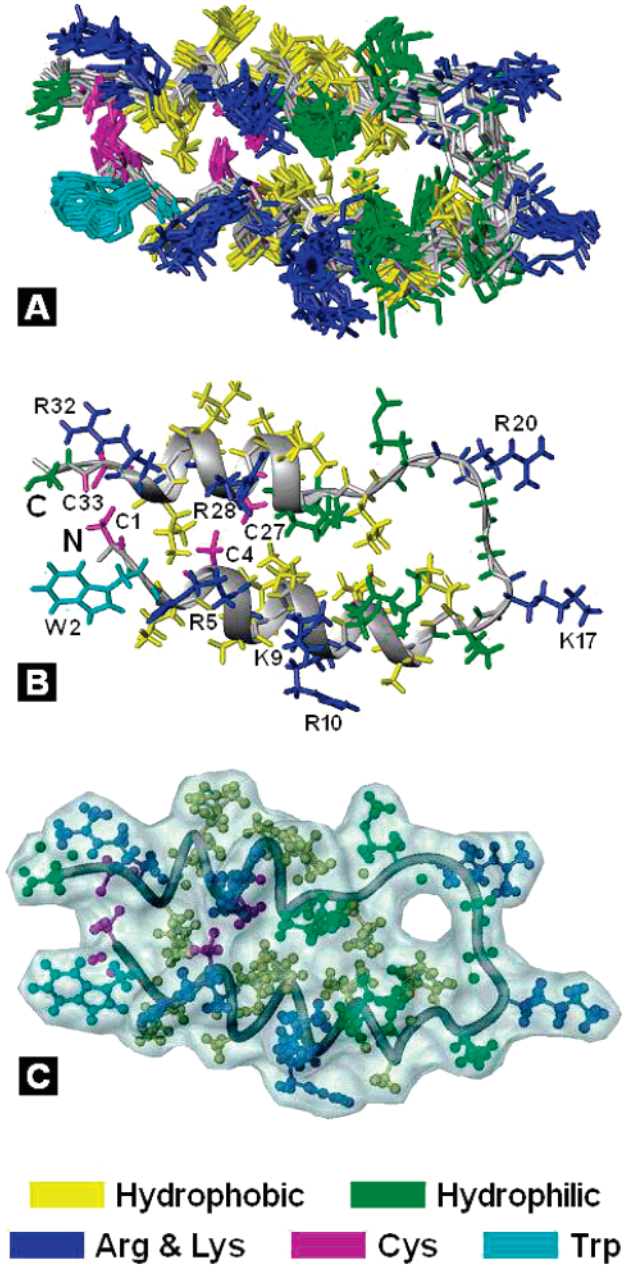

FIGURE 5: (A) Ensemble of 15 lowest energy structures of Mini-B_{ox} in SDS micelles. The backbone (gray) and the side-chain heavy atoms (colored) are shown; the hydrogen atoms are omitted for clarity. (B) Representative structure (closest to the mean structure of the ensemble) of Mini-B_{ox} in SDS. (C) Molecular surface formed by the structure. Panels A and B were prepared with MolMol (*59*);panel C was prepared with PPG (*67*).

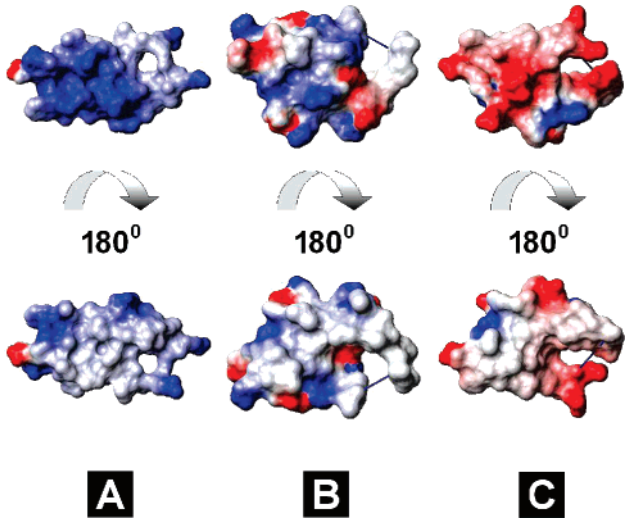

FIGURE 6: Electrostatic potential surface of Mini-B_{ox} (A) and the corresponding segments of NK-lysin (B) and saposin C (C). NK-lysin and saposin C segments are constructed from their PDB coordinates [1NKL (*34*) and 1SN6 (*33*), respectively]. Positively charged regions are blue, and negatively charged regions are red. The orientation of Mini-B_{ox} shown at the top of panel A is the same as the orientation used in Figure 5. This figure was prepared with MolMol (*59*).

This marked partitioning of hydrophobic residues to one face and positively charged residues to the opposite face is likely key in the mechanism by which Mini-B, and presumably SP-B, functions.

Tryptophan is an amino acid that typically either contributes to the hydrophobic core of a protein or, in lipid-associated proteins, it may "anchor" the protein to the polar/apolar interface. In Mini-B, the tryptophan side chain (Figure 5B) does not appear to take part in any interhelix interactions and therefore its role is most likely in interacting with lipids to help anchor Mini-B at the lipid−water interface. This role is consistent with the tryptophan's location between the hydrophobic face and the charged face of the 3D structure of Mini-B. A critical role for this tryptophan in positioning Mini-B and SP-B at the lipid interface is supported by previous studies that have found that Trp 9 of SP-B is critical for optimal interface affinity (*47*, *64*). It should be noted that although this tryptophan is at position 9 of SP-B, it is at position 2 of Mini-B and so it is conceivable, although unlikely, that it may take on a different structure when the first seven residues of SP-B are present.

The loop region of Mini-B is composed of part of the loop that connects helices 1 and 2 and part of the loop that connects helices 3 and 4 in full length SP-B. There are two positively charged residues in the loop of Mini-B (one from each of the parent loops of SP-B). In Mini-B this loop is unstructured, and it may be that these side chains are able to reconfigure in such a way as to interact optimally with lipid molecules. Since this loop is unstructured in Mini-B, it is clear that the loop itself is not forcing any nonnative contacts between the two helices. From the Mini-B structure it is not possible to draw any conclusions as to the characteristics of the corresponding loops in full length SP-B; they may also be unstructured, or they may take on a more defined conformation than the Mini-B loop.

The NMR spectra showed evidence that the structure of some regions of Mini-B_{ox} in SDS was dynamic on intermediate (on the order of milliseconds) and slower time scales. There were several weaker peaks in the HSQC spectra, likely representing minor conformations of residues 7, 18, and 22. These peaks did not lose intensity as the concentration of Mini-B was reduced, and thus it appears that protein−protein binding is not responsible for the minor conformations. Additionally, the intensity of the peaks originating from residues 1−5 was relatively low in the NMR spectra, in comparison to the peaks from other parts of the peptide. We interpret these spectral features as indicating a certain degree of plasticity in the regions of Mini-B covering the N-terminus, the N-terminal segment of the first helix, and the loop that connects the two helices. It is possible that this

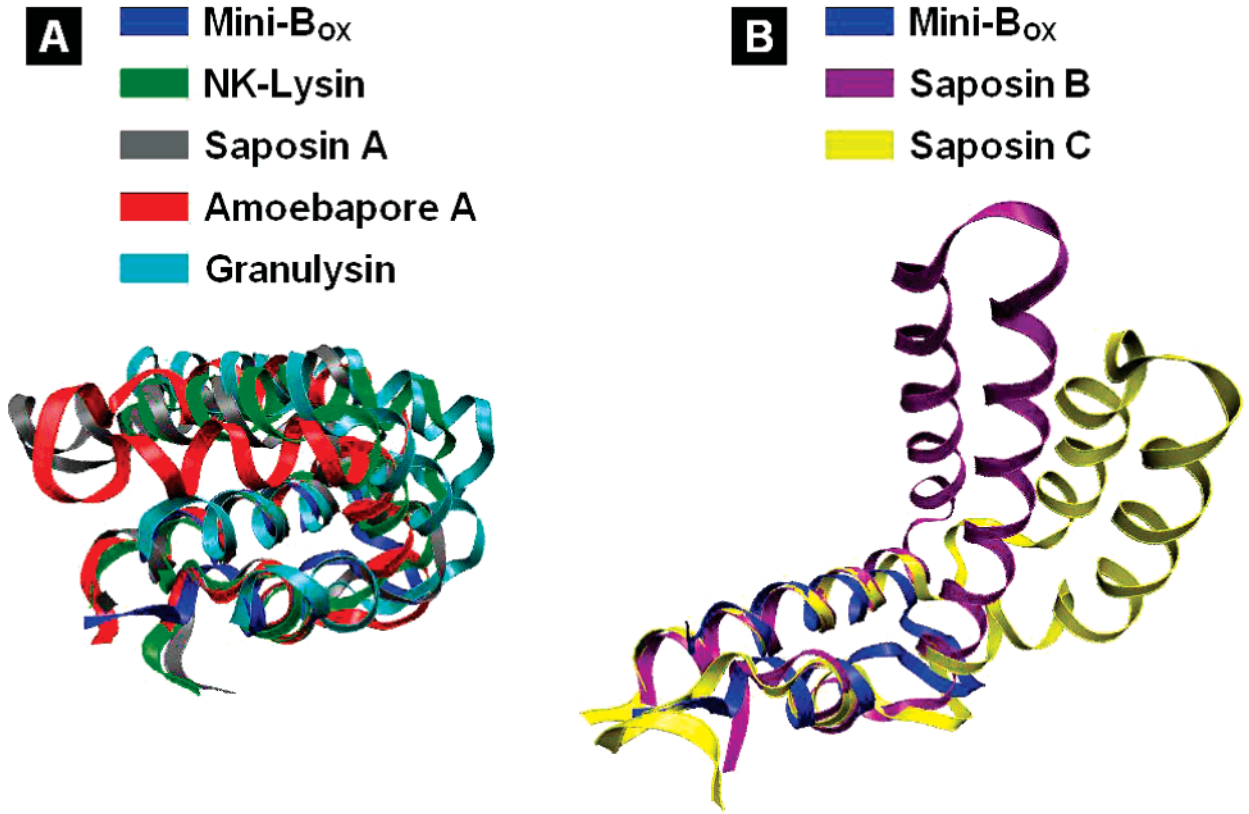

FIGURE 7: Overlay of the backbone structures of Mini-B_{ox} and other saposin family proteins. (A) Mini-B and closed-type saposins: NK-lysin (*34*), saposin A (*31*), amoebapore A (*35*), and granulysin (*36*). (B) Mini-B and open-type saposins: saposin B (*32*) and saposin C (*33*). This figure was prepared with VMD (*68*).

flexibility has a functional role, that is, to allow Mini-B to form different types of associations with lipids.

From diffusion NMR experiments (DOSY), it was possible to measure the hydrodynamic diameter of the SDS micelles and the Mini-B/SDS complexes. In the absence of Mini-B, the hydrodynamic diameter of the micelles was found to be 5.8 nm. When Mini-B was present, the hydrodynamic diameter of the complex was 6.8 nm. The positioning of Mini-B within the micelles was not defined by these studies (and will be a subject of future work), but given its structure, it is likely that Mini-B is positioned with its helices roughly parallel to the surface of the micelle, with its hydrophobic face in contact with the acyl chains of SDS and its positively charged face in contact with the SDS head groups and surrounding water. Such positioning is consistent with the observed increase in hydrodynamic diameter of the complex.

Several high-resolution structures have been determined for saposin proteins, the family to which SP-B belongs. These are saposin A (*31*), saposin B (*32*), saposin C (*33*), NK-lysin (*34*), and amoebapore A (*35*), as well as the saposin-related protein granulysin (*36*). All the saposin proteins form structures with four to five helices, with interactions between the N- and C-terminal helices stabilized by two disulfide bonds and interactions between the middle helices stabilized by a third disulfide bond (Figure 1). However, the structures differ significantly in how the N- and C-terminal helix pair (which corresponds to the region covered by Mini-B) interacts with the middle helix pair. In some proteins, such as saposin A, NK-lysin, amoebapore A, and granulysin, the two helix pairs pack together tightly into a "closed" overall structure (Figure 7A). On the other hand, in saposins B and C, the pairs of helices do not pack closely together and the overall tertiary structure is relatively "open" (Figure 7B). In saposin B, the open-type structure results in the formation of a large hydrophobic cavity that is likely responsible for saposin B's ability to extract target lipids from membranes (*32*). Saposin C, in complex with SDS micelles, also possesses an exposed hydrophobic pocket that is implicated in interactions with lipids (*33*). Figure 6 shows the electrostatic surfaces for Mini-B and, for comparison, the corresponding regions of NK-lysin, as a representative of the closed-type saposin structure, and saposin C, as a representative of the open type saposin structure. The surfaces on the bottom row of Figure 6 represent the face of the helix pair that is positioned to interact with the rest of the protein. Mini-B more resembles the saposin C helix pair, which exhibits a primarily hydrophilic face and a primarily hydrophobic face, than it does the NK-lysin structure, which exhibits a much less extensive hydrophobic patch.

SP-B has been observed to exhibit a number of in vitro behaviors relating to its interactions with lipids, such as promoting phospholipid vesicle aggregation, fusion, and lysis, promoting rapid adsorption of surfactant material to an air−water interface, and promoting readsorption of surfactant material to the interface during compression−expansion cycling (*16*). These in vitro activities relate to three important properties of lung surfactant activity in vivo: rapid interfacial absorption, surface tension reduction during compression, and respreading of the surface film during subsequent expansion. A number of potential molecular mechanisms for SP-B's essential contributions to these critical lung surfactant properties have been proposed (*65*). SP-B may act as a bridge

between bilayers and/or between bilayers and monolayers to keep components that are squeezed out during compression in close association with the interface for rapid respreading. SP-B may stabilize high-energy intermediates required for phospholipids to pass into the interfacial monolayer. SP-B may induce lipid-packing perturbations leading to transfer of surfactant material to the interface. SP-B may act as a sort of carrier, taking associating molecules with it to the interface. The structure of Mini-B in SDS, with its strongly amphipathic surface and projecting tryptophan anchor, appears very well suited for making strong interactions with lipids, especially anionic species, at an interface. The hydrophobic face provides a surface for interactions with several lipid acyl chains, the positively charged face provides a surface for interactions with negatively charged lipid head groups, and the tryptophan side chain, which is itself amphipathic, extends out from the surface in a position to anchor Mini-B at the interface. The relatively large extent of the positively charged patch suggests that this surface may be able to interact with a second lipid layer through electrostatic interactions, or at least reduce the electrostatic repulsion between negatively charged lipid layers, allowing them to stay in closer association.

Mini-B is considerably more effective in rat lung oxygenation and dynamic compliance assays than its unlinked N- and C-terminal halves, even when they are added together (*49*). This indicates that there is indeed extra functionality associated with Mini-B's relatively large hydrophobic and cationic surfaces. Now that Mini-B's structure and resonance frequency assignments are known, it will be possible in future studies to directly observe Mini-B's interactions with phospholipids and other proteins. In particular, it will be of interest to study Mini-B's structure and lipid interactions in more physiologically relevant systems than SDS micelles, such as phospholipid monolayers and bilayers.

ACKNOWLEDGMENT

We thank Brian Dawson and Health Canada for acquiring some of the NMR data used in these studies. We acknowledge the Canadian National High Field NMR Centre (NANUC) for their assistance and use of the facilities. Operation of NANUC is funded by the Canadian Institutes of Health Research, the Natural Science and Engineering Research Council of Canada, and the University of Alberta. We also thank Tran-Chin Yang for the DOSY studies of SDS micelles and Stéphan Dubrau for help with preparing Figure 4.

SUPPORTING INFORMATION AVAILABLE

Two-dimensional $^{15}N-^{1}H$ HSQC spectra of Mini-B at 1.5, 0.5, and 0.1 mM concentrations and 2D DOSY spectra of Mini-B. This material is available free of charge via the Internet at http://pubs.acs.org.

REFERENCES

1. von Neergaard, K. (1929) Neue Auffassungen über einen Grundbegriff der Atemmechanik. Die Retraktionskraft der Lunge, abhangig von der Oberflachenspannung in den Alveolem, *Z. Gesamte Exp. Med. 66*, 373−394.
2. Clements, J. A. (1957) Surface tension of lung extracts, *Proc. Soc. Exp. Biol. Med. 95*, 170−172.
3. Crouch, E., and Wright, J. R. (2001) Surfactant proteins a and d and pulmonary host defense, *Annu. Rev. Physiol. 63*, 521−554.
4. Hallman, M., Glumoff, V., and Ramet, M. (2001) Surfactant in respiratory distress syndrome and lung injury, *Comp. Biochem. Physiol., Part A: Mol. Integr. Physiol. 129*, 287−294.
5. Seeger, W., Gunther, A., Walmrath, H. D., Grimminger, F., and Lasch, H. G. (1993) Alveolar surfactant and adult respiratory distress syndrome. Pathogenetic role and therapeutic prospects, *Clin. Invest. 71*, 177−190.
6. Schwartz, R. M., Luby, A. M., Scanlon, J. W., and Kellogg, R. J. (1994) Effect of surfactant on morbidity, mortality, and resource use in newborn infants weighing 500 to 1500 g, *N. Engl. J. Med. 330*, 1476−1480.
7. Gunther, A., Ruppert, C., Schmidt, R., Markart, P., Grimminger, F., Walmrath, D., and Seeger, W. (2001) Surfactant alteration and replacement in acute respiratory distress syndrome, *Respir. Res. 2*, 353−364.
8. Lewis, J. F., and Veldhuizen, R. (2003) The role of exogenous surfactant in the treatment of acute lung injury, *Annu. Rev. Physiol. 65*, 613−642.
9. Nogee, L. M., Garnier, G., Dietz, H. C., Singer, L., Murphy, A. M., deMello, D. E., and Colten, H. R. (1994) A mutation in the surfactant protein B gene responsible for fatal neonatal respiratory disease in multiple kindreds, *J. Clin. Invest. 93*, 1860−1863.
10. Clark, J. C., Wert, S. E., Bachurski, C. J., Stahlman, M. T., Stripp, B. R., Weaver, T. E., and Whitsett, J. A. (1995) Targeted disruption of the surfactant protein B gene disrupts surfactant homeostasis, causing respiratory failure in newborn mice, *Proc. Natl. Acad. Sci. U.S.A. 92*, 7794−7798.
11. Johansson, J., and Curstedt, T. (1997) Molecular structures and interactions of pulmonary surfactant components, *Eur. J. Biochem. 244*, 675−693.
12. Lang, C. J., Daniels, C. B., and Orgeig, S. (2005) New insights into the thermal dynamics of the Surfactant system from warm and cold animals, in *Lung Surfactant Function and Disorder*, pp 17−57, Taylor & Francis Group, Boca Raton, FL.
13. Perez-Gil, J. (2002) Molecular interactions in pulmonary surfactant films, *Biol. Neonate 81* (Suppl. 1), 6−15.
14. McCormack, F. X. (1998) Structure, processing and properties of surfactant protein A, *Biochim. Biophys. Acta 1408*, 109−131.
15. Crouch, E. C. (1998) Structure, biologic properties, and expression of surfactant protein D (SP-D), *Biochim. Biophys. Acta 1408*, 278−289.
16. Hawgood, S., Derrick, M., and Poulain, F. (1998) Structure and properties of surfactant protein B, *Biochim. Biophys. Acta 1408*, 150−160.
17. Johansson, J. (1998) Structure and properties of surfactant protein C, *Biochim. Biophys. Acta 1408*, 161−172.
18. Hamvas, A., Cole, F. S., deMello, D. E., Moxley, M., Whitsett, J. A., Colten, H. R., and Nogee, L. M. (1994) Surfactant protein B deficiency: antenatal diagnosis and prospective treatment with surfactant replacement, *J. Pediatr. 125*, 356−361.
19. Robertson, B., Kobayashi, T., Ganzuka, M., Grossmann, G., Li, W. Z., and Suzuki, Y. (1991) Experimental neonatal respiratory failure induced by a monoclonal antibody to the hydrophobic surfactant-associated protein SP-B, *Pediatr. Res. 30*, 239−243.
20. Possmayer, F. (1988) A proposed nomenclature for pulmonary surfactant-associated proteins, *Am. Rev. Respir. Dis. 138*, 990−998.
21. Longo, M. L., Bisagno, A. M., Zasadzinski, J. A., Bruni, R., and Waring, A. J. (1993) A function of lung surfactant protein SP-B, *Science 261*, 453−456.
22. Baatz, J. E., Elledge, B., and Whitsett, J. A. (1990) Surfactant protein SP-B induces ordering at the surface of model membrane bilayers, *Biochemistry 29*, 6714−6720.
23. Perez-Gil, J., Casals, C., and Marsh, D. (1995) Interactions of hydrophobic lung surfactant proteins SP-B and SP-C with dipalmitoylphosphatidylcholine and dipalmitoylphosphatidylglycerol bilayers studied by electron spin resonance spectroscopy, *Biochemistry 34*, 3964−3971.
24. Lipp, M. M., Lee, K. Y., Zasadzinski, J. A., and Waring, A. J. (1996) Phase and morphology changes in lipid monolayers induced by SP-B protein and its amino-terminal peptide, *Science 273*, 1196−1199.
25. Lipp, M. M., Lee, K. Y. C., Takamoto, D. Y., Zasadzinski, A. J., and Waring, A. J. (1998) Co-existence of buckled and flat monolayers, *Phys. Rev. Lett. 81*, 1650−1653.
26. Ding, J., Doudevski, I., Warriner, H. E., Alig, T., Zasadzinki, J. A., Waring, A. J., and Sherman, M. A. (2003) Nanostructure changes in lung surfactant monolayers induced by interactions

between palmitoyloleoylphosphatidylglycerol and surfactant protein B,. *Langmuir 19*, 1539−1550.
27. Suzuki, Y., Fujita, Y., and Kogishi, K. (1989) Reconstitution of tubular myelin from synthetic lipids and proteins associated with pig pulmonary surfactant, *Am. Rev. Respir. Dis. 140*, 75−81.
28. Williams, M. C., Hawgood, S., and Hamilton, R. L. (1991) Changes in lipid structure produced by surfactant proteins SP-A, SP-B, and SP-C, *Am. J. Respir. Cell Mol. Biol. 5*, 41−50.
29. Beck, D. C., Na, C. L., Whitsett, J. A., and Weaver, T. E. (2000) Ablation of a critical surfactant protein B intramolecular disulfide bond in transgenic mice, *J. Biol. Chem. 275*, 3371−3376.
30. Zaltash, S., Palmblad, M., Curstedt, T., Johansson, J., and Persson, B. (2000) Pulmonary surfactant protein B: a structural model and a functional analogue, *Biochim. Biophys. Acta 1466*, 179−186.
31. Ahn, V. E., Leyko, P., Alattia, J. R., Chen, L., and Prive, G. G. (2006) Crystal structures of saposins A and C, *Protein Sci. 15*, 1849−1857.
32. Ahn, V. E., Faull, K. F., Whitelegge, J. P., Fluharty, A. L., and Prive, G. G. (2003) Crystal structure of saposin B reveals a dimeric shell for lipid binding, *Proc. Natl. Acad. Sci. U.S.A. 100*, 38−43.
33. Hawkins, C. A., de Alba, E., and Tjandra, N. (2005) Solution structure of human saposin C in a detergent environment, *J. Mol. Biol. 346*, 1381−1392.
34. Liepinsh, E., Andersson, M., Ruysschaert, J. M., and Otting, G. (1997) Saposin fold revealed by the NMR structure of NK-lysin, *Nat. Struct. Biol. 4*, 793−795.
35. Hecht, O., Van Nuland, N. A., Schleinkofer, K., Dingley, A. J., Bruhn, H., Leippe, M., and Grotzinger, J. (2004) Solution structure of the pore-forming protein of *Entamoeba histolytica*, *J. Biol. Chem. 279*, 17834−17841.
36. Anderson, D. H., Sawaya, M. R., Cascio, D., Ernst, W., Modlin, R., Krensky, A., and Eisenberg, D. (2003) Granulysin crystal structure and a structure-derived lytic mechanism, *J. Mol. Biol. 325*, 355−365.
37. Power, J. H., Doyle, I. R., Davidson, K., and Nicholas, T. E. (1999) Ultrastructural and protein analysis of surfactant in the Australian lungfish *Neoceratodus forsteri*: evidence for conservation of composition for 300 million years, *J. Exp. Biol. 202*, 2543−2550.
38. Vandenbussche, G., Clercx, A., Clercx, M., Curstedt, T., Johansson, J., Jornvall, H., and Ruysschaert, J. M. (1992) Secondary structure and orientation of the surfactant protein SP-B in a lipid environment. A Fourier transform infrared spectroscopy study, *Biochemistry 31*, 9169−9176.
39. Pastrana-Rios, B., Taneva, S., Keough, K. M., Mautone, A. J., and Mendelsohn, R. (1995) External reflection absorption infrared spectroscopy study of lung surfactant proteins SP-B and SP-C in phospholipid monolayers at the air/water interface, *Biophys. J. 69*, 2531−2540.
40. Cruz, A., Casals, C., and Perez-Gil, J. (1995) Conformational flexibility of pulmonary surfactant proteins SP-B and SP-C, studied in aqueous organic solvents, *Biochim. Biophys. Acta 1255*, 68−76.
41. Revak, S. D., Merritt, T. A., Hallman, M., Heldt, G., La Polla, R. J., Hoey, K., Houghten, R. A., and Cochrane, C. G. (1991) The use of synthetic peptides in the formation of biophysically and biologically active pulmonary surfactants, *Pediatr. Res. 29*, 460−465.
42. Walther, F. J., Hernandez-Juviel, J. M., Gordon, L. M., Sherman, M. A., and Waring, A. J. (2002) Dimeric surfactant protein B peptide SP-B 1−25 in neonatal and acute respiratory distress syndrome, *Exp. Lung Res. 28*, 623−640.
43. Veldhuizen, E. J., Waring, A. J., Walther, F. J., Batenburg, J. J., van Golde, L. M., and Haagsman, H. P. (2000) Dimeric N-terminal segment of human surfactant protein B (dSP-B(1−25)) has enhanced surface properties compared to monomeric SP-B(1−25), *Biophys. J. 79*, 377−384.
44. Tanaka, Y., Takei, T., Aiba, T., Masuda, K., Kiuchi, A., and Fujiwara, T. (1986) Development of synthetic lung surfactants, *J. Lipid Res. 27*, 475−485.
45. Kang, J. H., Lee, M. K., Kim, K. L., and Hahm, K. S. (1996) The relationships between biophysical activity and the secondary structure of synthetic peptides from the pulmonary surfactant protein SP-B, *Biochem. Mol. Biol. Int. 40*, 617−627.
46. Baatz, J. E., Sarin, V., Absolom, D. R., Baxter, C., and Whitsett, J. A. (1991) Effects of surfactant-associated protein SP-B synthetic analogs on the structure and surface activity of model membrane bilayers, *Chem. Phys. Lipids 60*, 163−178.
47. Ryan, M. A., Qi, X., Serrano, A. G., Ikegami, M., Perez-Gil, J., Johansson, J., and Weaver, T. E. (2005) Mapping and analysis of the lytic and fusogenic domains of surfactant protein B, *Biochemistry 44*, 861−872.
48. Wiswell, T. E., Knight, G. R., Finer, N. N., Donn, S. M., Desai, H., Walsh, W. F., Sekar, K. C., Bernstein, G., Keszler, M., Visser, V. E., Merritt, T. A., Mannino, F. L., Mastrioianni, L., Marcy, B., Revak, S. D., Tsai, H., and Cochrane, C. G. (2002) A multicenter, randomized, controlled trial comparing Surfaxin (Lucinactant) lavage with standard care for treatment of meconium aspiration syndrome, *Pediatrics 109*, 1081−1087.
49. Waring, A. J., Walther, F. J., Gordon, L. M., Hernandez-Juviel, J. M., Hong, T., Sherman, M. A., Alonso, C., Alig, T., Braun, A., Bacon, D., and Zasadzinski, J. A. (2005) The role of charged amphipathic helices in the structure and function of surfactant protein B, *J. Pept. Res. 66*, 364−374.
50. Kurutz, J. W., and Lee, K. Y. (2002) NMR structure of lung surfactant peptide SP-B(11−25), *Biochemistry 41*, 9627−9636.
51. Booth, V., Waring, A. J., Walther, F. J., and Keough, K. M. (2004) NMR structures of the C-terminal segment of surfactant protein B in detergent micelles and hexafluoro-2-propanol, *Biochemistry 43*, 15187−15194.
52. Fields, C. G., Lloyd, D. H., Macdonald, R. L., Otteson, K. M., and Noble, R. L. (1991) HBTU activation for automated Fmoc solid-phase peptide synthesis, *Pept. Res. 4*, 95−101.
53. Morris, K. F., and Johnson, C. S. (1992) Diffusion-ordered two-dimensional nuclear magnetic resonance spectroscopy, *J. Am. Chem. Soc. 114* (8), 3139−3141.
54. Tanner, J. E. (1970) Use of the stimulated echo in NMR diffusion studies, *J. Chem. Phys. 52*, 2523−2526.
55. Sklenár, V., Piotto, M., Leppik, R., and Saudek, V. (1993) Gradient-tailored water suppression for proton-nitrogen-15 HSQC experiments optimized to retain full sensitivity, *J. Magn. Reson. 102*, 241−245.
56. Delaglio, F., Grzesiek, S., Vuister, G. W., Zhu, G., Pfeifer, J., and Bax, A. (1995) NMRPipe: a multidimensional spectral processing system based on UNIX pipes, *J. Biomol. NMR 6*, 277−293.
57. Goddard, T. D., and Kneller, D. G. Sparky 3, University of California, San Francisco, CA.
58. Brunger, A. T., Adams, P. D., Clore, G. M., DeLano, W. L., Gros, P., Grosse-Kunstleve, R. W., Jiang, J. S., Kuszewski, J., Nilges, M., Pannu, N. S., Read, R. J., Rice, L. M., Simonson, T., and Warren, G. L. (1998) Crystallography & NMR system: A new software suite for macromolecular structure determination, *Acta Crystallogr. D: Biol. Crystallogr. 54*, 905−921.
59. Koradi, R., Billeter, M., and Wuthrich, K. (1996) MOLMOL: a program for display and analysis of macromolecular structures, *J. Mol. Graphics 14* (51−55−.
60. Hayter, J. B., and Penfold, J. (1981) Self-consistent structural and dynamic study of concentrated micelle solutions, *J. Chem. Soc., Faraday Trans. 1 77*, 1851−1863.
61. Sheu, E. Y., Wu, C. F., Chen, S. H., and Blum, L. (1985) Application of a rescaled mean spherical approximation to strongly interacting ionic micellar solutions, *Phys. Rev. A 32*, 3807−3810.
62. Itri, R., and Amaral, L. Q. (1991) Distance distribution function of sodium dodecyl sulfate micelles by X-ray scattering, *J. Phys. Chem. 95*, 423−427.
63. Serrano, A. G., Cruz, A., Rodriguez-Capote, K., Possmayer, F., and Perez-Gil, J. (2005) Intrinsic structural and functional determinants within the amino acid sequence of mature pulmonary surfactant protein SP-B, *Biochemistry 44*, 417−430.
64. Serrano, A. G., Ryan, M., Weaver, T. E., and Perez-Gil, J. (2006) Critical structure-function determinants within the N-terminal region of pulmonary surfactant protein SP-B, *Biophys. J. 90*, 238−249.
65. Serrano, A. G., and Perez-Gil, J. (2006) Protein-lipid interactions and surface activity in the pulmonary surfactant system, *Chem. Phys. Lipids 141*, 105−118.
66. Wishart, D. S., and Nip, A. M. (1998) Protein chemical shift analysis: a practical guide, *Biochem. Cell Biol. 76*, 153−163.
67. Sanner, M. F., Olson, A. J., and Spehner, J. C. (1996) Reduced surface: an efficient way to compute molecular surfaces, *Biopolymers 38*, 305−320.
68. Humphrey, W., Dalke, A., and Schulten, K. (1996) VMD: visual molecular dynamics, *J. Mol. Graphics 14* 33−38.

BI7011756